Using the stochastic-threshold incision model to understand the tectonic expression on fluvial topography: theory and application to the Dadu River basin, eastern Tibetan Plateau

Yizhou Wang, Dewen Zheng, and Huiping Zhang

State Key Laboratory of Earthquake Dynamics, Institute of Geology, China Earthquake Administration, Beijing 100029, China

Corresponding author: Yizhou Wang (wangyizhou2016@outlook.com)

Key Points:

- Assuming timely dependent tectonic uplift, we present an analytic solution to the linear stochastic-threshold incision model equation.
- The analytic solution yields a linear inverse scheme to decipher tectonic uplift rate history from river longitudinal profiles.
- Two-phase increase in the uplift/incision rates that initiated at the late Miocene and early Pleistocene was inferred for the Dadu basin.

Abstract

The non-linear reliance of channel steepness on erosion rates can be reconciled by the stochastic-threshold incision model that incorporates river incision threshold and discharge probability distribution into erosion efficiency. Here, we explored the usage of the model in river longitudinal profile inversion, by assuming time-dependent tectonic forcing and a linear exponent that relates channel incision to slope. We developed an analytical solution to the model equation and an inverse scheme to retrieve relative uplift rate history, whose validity was based on the theoretical demonstration on knickpoint preservation. Application of the inverse scheme to the main trunks of the Dadu River basin in the eastern Tibetan Plateau produced a history with two-phase increases in the uplift/incision rates, which is similar to the results from low-temperature thermochronology. Thus, our analytical procedures provide new insights into the link of tectonic uplift and river profile evolution, when channel steepness depends on erosion rates non-linearly.

Keywords: stochastic-threshold incision model, time-dependent tectonic uplift, linear slope exponent, analytical solution, inverse scheme

Plain Language Summary

River incision into channel bedrock occurs only when the stream power generated by large floods overcomes the critical value of shear stress. Despite the assumption of a linear dependency of river erosion on channel gradients, the linear stochastic-threshold incision model that incorporates both incision threshold and runoff variability can predict the monotonic, non-linear increase of channel steepness with erosion rates. Channel steepness measures the slope normalized for drainage area. Considering time-dependent tectonic uplift, we presented an analytical solution to the linear stochastic-threshold model equation and derived an inversion scheme to decode the temporary changes in the relative uplift rates from river long profiles. The inverse scheme was successfully applied to the Dadu River that flows through the eastern margin of the Tibetan Plateau. Our analytical work thus helps to decipher the expression of active tectonics in erosional landscapes.

1 Introduction

In active mountain ranges, the fluvial system evolves as a response to the spatiotemporal changes in both tectonic and climatic forcing [Howard and Kerby, 1983; Whipple and Tucker, 1999]. The fluvial channels adjust their profile shape by modulating the pattern of erosion and sediment transport, exerting a first control on orogen-scale relief [Whipple and Tucker, 2002; Kirby and Whipple, 2012]. Since decades, a great many models have been proposed to link the processes between tectonic uplift, climate change, river incision, and landscape evolution [e.g. Howard and Kerby, 1983; Howard, 1994; Johnson and Whipple, 2007; Lague, 2014]. Instead of relating to the physics of specific incision process, the stream-power incision model (SPIM) presents the channel bedrock incision rate, E [L/T], in terms of channel slope, S [L/L], and upstream drainage area, A [L^2] [Howard and Kerby, 1983]:

$$\frac{\partial z(t,x)}{\partial t} = U(t,x) - E(t,x) = U(t,x) - KA^m \left[\frac{\partial z(t,x)}{\partial x}\right]^n \quad (1)$$

where U [L/T] is tectonic uplift rate, z [L] is channel elevation, x [L] is horizontal upstream distance along the channel, $S = \partial z/\partial x$ is channel slope, t [T] is time, and K [L^{1-2m}/T] is channel erodibility coefficient. m and n are positive exponents that measure the significance of drainage area and slope to erosion, respectively.

Although numerical solutions to Equation (1) usually have been used in landscape evolution forward models [e.g. Tucker et al., 2001; Refice et al., 2012], inversion on the river long profiles calls for analytical solutions to the SPIM equation [Pritchard et al., 2009; Goren et al., 2014, 2021]. Assuming a linear erosion–slope relationship, i.e. $n = 1$, analytical solutions to Equation (1) were derived and the related inversion schemes were developed to infer the climatic and/or tectonic conditions in many active landscapes [Goren et al., 2014; Rudge et al., 2015; Goren, 2016]. However, a growing body of evidences, at both the regional and global scales, have shown non-linear relationships between erosion rates and channel steepness that measures channel gradients normalized for downstream increases in drainage area [e.g. Harkins et al., 2007; Harel et al., 2016; Hilley et al., 2019]. These findings thus questions the validity of the routinely used linear assumption ($n = 1$). Combing $n \neq 1$ and timely variable tectonic uplift, analytical solutions to Equation (1) predicts the formation of stretch zones that contains no tectonic information and consuming and merging knickpoints where the tectonic signals could partly and even entirely lost [Royden and Perron, 2013; Wang et al., 2022]. The non-linear dynamics thus hinder formal attempts to relate the channel profile form to tectonic history.

Alternatively, many studies have found that the non-linear erosion–steepness scaling does not necessarily require a non-linear slope exponent n [Snyder et al., 2003; Lague et al., 2005; Dibiase and Whipple, 2011]. Rather, even if using $n = 1$, the observed relation of non-linear increase of channel steepness with increasing erosion rate can well be reconciled by taking the effects of both bedrock resistance to erosion and the effectiveness of stream power [Whipple, 2009; Scherler et al., 2017]. These studies emphasized that river incision was actually triggered by large floods that generates high stream power to overcome the channel substrate detachment thresholds, which is not presented in the simple SPIM (Equation 1).

In this contribution, we followed DiBiase and Whipple [2011] to construct the transient equation of the stochastic-threshold incision model (STIM) that incorporates both the incision threshold and discharge distribution function. Then, by assuming a timely dependent $U(t)$ and linear n, we derived an analytical solution to the STIM equation and presented an inversion scheme to infer $U(t)$ from river long profiles. As a case study, we applied the inverse scheme to the Dadu River basin that drains parts of the eastern Tibetan Plateau.

2 A mathematical expression of the stochastic-threshold incision model (STIM)

Stream power incision into the detachment-limited channel bed occurs when the bed shear stress, τ [Pa], overcome a critical value (τ_c). The instantaneous vertical incision rate, I, scales with τ in the term of a power-law function [Howard and Kerby, 1983]:

$$I = k_e \cdot (\tau^a - \tau_c^a) \quad (2)$$

where k_e quantifies the channel substrate resistance to incision and a depends on specific incision mechanism. Following the assumptions of steady, uniform flow and negligible bank friction [Howard, 1994], Dibiase and Whipple [2011] defined τ as:

$$\tau = k_t \cdot (\frac{Q}{w})^{\alpha} \cdot (\frac{\partial z}{\partial x})^{\beta} \quad (3)$$

where k_t is a constant that incorporates water density, gravitational and frictional terms, Q [L^3/T] is river discharge, and w [L] is channel width, and α and β are positive exponents. Hydrologic records or field measurements support a power-law to relate bankfull channel width (w_b) to mean-annual discharge ($\bar{Q}$) [Montgomery and Gran, 2001; Zhang et al., 2017]:

$$w_b = k_w \bar{Q}^{\omega_b} \quad (4)$$

where k_w and ω_b are empirical scaling parameters. To incorporate the stochastic distribution of discharge into bed shear stress (Equation 3), we followed Scherler et al. [2017] to adopt a geometrical treatment that channel width (w) changes as a function of discharge (Q):

$$\frac{w}{w_b} = (\frac{Q}{\bar{Q}})^{\omega_s} \quad (5)$$

where ω_s is also an empirical scaling parameter. Mean-annual discharge ($\bar{Q}$) usually correlates with drainage area [Tucker, 2004]:

$$\bar{Q} = R_b A^c \quad (6)$$

where c is positive exponent and R_b (L/T) represents mean annual catchment-integrated runoff. Assigning Equations (3-6) into (2), we derived:

$$I = k_e k_t^a k_w^{-\alpha a} R_b^{\alpha a(1-\omega_b)} \cdot (\frac{Q}{\bar{Q}})^{\alpha a(1-\omega_s)} \cdot A^{\alpha a c(1-\omega_b)} \cdot (\frac{\partial z}{\partial x})^{\beta a} - k_e \tau_c^a \quad (7)$$

To make Equation (7) concise, we followed Dibiase and Whipple [2011] to define four variables, $\kappa = k_e k_t^a k_w^{-\alpha a} R_b^{\alpha a(1-\omega_b)}$, $\gamma = \alpha a(1-\omega_s)$, $\Psi = k_e \tau_c^a$, and $Q^* = \frac{Q}{\bar{Q}}$. Q^* is normalized discharge. In the simple form of the SPIM (Equation 1), $m = \alpha a(1-\omega_b)$ and $n = \beta a$. Thus, Equation (7) can be written as:

$$I = \kappa \cdot (Q^*)^{\gamma} \cdot A^{cm} \cdot (\frac{\partial z}{\partial x})^n - \Psi \quad (8)$$

The probability density function (PDF) of normalized discharge (Q^*) can be defined as [Lague et al., 2005]:

$$\mathrm{PDF}(Q^*) = \frac{k^{k+1}}{\Gamma(k+1)} e^{-k/Q^*} Q^{*-(k+2)} \quad (9)$$

where Γ is the gama function, and k is the discharge variability parameter. The long-term erosion rate ($E_{s\text{-}c}$) that incorporates the stochastic distribution of discharge thus can be produced by integrating I over the range of all possible discharges:

$$E_{s-c} = \int_{Q_c^*}^{Q_m^*} [\kappa \cdot (Q^*)^{\gamma} \cdot A^{cm} \cdot (\frac{\partial z}{\partial x})^n - \Psi] \cdot \frac{k^{k+1}}{\Gamma(k+1)} e^{-k/Q^*} Q^{*-(k+2)} dQ^* \quad (10)$$

where $Q_m^* = Q_m/\bar{Q}$ and $Q_c^* = Q_c/\bar{Q}$. Q_m is the maximum possible discharge and Q_c is the critical discharge to overcome the threshold shear stress. As long as Q_m is sufficiently large, the integration of Equation (10) is insensitive to the choice of Q_m [Lague et al., 2005]. Equation (10) contains two terms, one of which represents stream power incision (E_s) and another relates to erosion thresholds (E_c):

$$E_s = K' \cdot A^{cm} \cdot (\frac{\partial z}{\partial x})^n \quad (11)$$

$$E_c = \Psi \cdot \frac{k^{k+1}}{\Gamma(k+1)} \cdot \int_{Q_c^*}^{Q_m^*} e^{-k/Q^*} Q^{*-(k+2)}\, dQ^* \quad (12)$$

where $K' = \kappa \cdot \frac{k^{k+1}}{\Gamma(k+1)} \cdot \int_{Q_c^*}^{Q_m^*} (Q^*)^{\gamma-(k+2)} \cdot e^{-k/Q^*} dQ^*$ depends on the critical discharge Q_c^*. If assuming $c = 1$ and neglecting the effects of incision threshold (i.e. $E_c = 0$), Equation (10) reduces to the simple form of incision rate (E) in Equation (1). We replaced E with $E_{s\text{-}c}$ in Equation (1):

$$\frac{\partial z}{\partial t} = U(t,x) - K'(Q_c^*) \cdot A^{cm} \cdot (\frac{\partial z}{\partial x})^n + E_c(Q_c^*) \quad (13)$$

Equation (13) is the mathematical form of the stochastic-threshold incision model (STIM).

3 Analytical description of the STIM equation

3.1 An integral approach to the steady-state form of the model equation

Assuming a balance between uplift rates and long-term erosion rates, i.e. Equation (13) equals to zero, we derived:

$$U(x) = K'(Q_c^*) \cdot A^{cm} \cdot S^n - E_c(Q_c^*) \text{ or } S = A^{-cm/n} \cdot [\frac{U(x)+E_c(Q_c^*)}{K\prime(Q_c^*)}]^{1/n} \quad (14)$$

If under the spatially uniform uplift pattern, i.e. $U(x) = U$, the incision efficiency and threshold related parameters, also should be constants along the river profile, i.e.$E_c(Q_c^*) = E_c$and $K'(Q_c^*) = K'$. Thus, Equation (14) reduces to:

$$S = A^{-cm/n} \cdot (\frac{U+E_c}{K\prime})^{1/n} \quad (15)$$

Equation (15) has the same form of the slope-area scaling for a graded river profile [Howard and Kerby, 1983]. Here, channel concavity $\theta = cm/n$ and steepness $k_s = (\frac{U+E_c}{K\prime})^{1/n}$.

Performing the integration in the upstream direction yields an analytical solution to Equation (15):

$$z = z_b + (\frac{U+E_c}{K\prime})^{1/n} \cdot (\frac{1}{A_0})^{cm/n} \cdot \varphi(x) \quad (16)$$

$$\text{with } \varphi(x) = \int_0^x [\frac{A_0}{A(x\prime)}]^{cm/n} dx' \quad (17)$$

where z_b is elevation of the base level and A_0 is a reference drainage area. Accordingly, Equations (16-17) produces a $\varphi - z$ plot, which is similar to the $\chi - z$ plot when $c = 1$ [Perron and Royden, 2013].

The steady-state form produces a way to determine the normalized critical discharge Q_c^*. Assigning Equation (15) into (8) and setting $I = 0$ yields [Dibiase and Whipple, 2011]:

$$Q_c^* = (\frac{\Psi}{\kappa \cdot k_s^n})^{1/\gamma} \quad (18)$$

3.2 A closed form analytical solution to the linear transient equation

By adopting $n = 1$ ($a = 3/2$ and $\beta = 2/3$ [Dibiase and Whipple, 2011]) and timely dependent uplift rate $U(t)$, Equation (13) can be re-arranged as:

$$\frac{\partial z}{\partial t} + K'(Q_c^*) \cdot A^{cm} \cdot \frac{\partial z}{\partial x} = U(t) + E_c(Q_c^*) \quad (19)$$

In the transient equation, K' and E_c are the functions of critical discharge that relates to channel steepness. It means that both K' and E_c can vary with $U(t)$. Thus, Equation (19) is difficult to be solved, if focusing on the whole river profile. Instead, we followed Wang et al. [2022] to deal with separate transient knickpoints.

The elevation change of a knickpoint that formed as a response to the change in tectonic uplift rates can be expressed as:

$$\frac{dz(t,x)}{dt} = \frac{\partial z}{\partial t} + \frac{\partial z}{\partial x} \cdot \frac{dx}{dx} \quad (20)$$

Compared with Equation (19), we can derive two characteristic equations:

$$\frac{dx}{dt} = K'(Q_c^*) \cdot A^{cm} \quad (21)$$

$$\frac{dz}{dt} = U(t) + E_c(Q_c^*) \quad (22)$$

Notably, it is unlike the condition of Equation (1) where incision efficiency keeps a constant through both time and space. In that case, all the knickpoints share a common retreat velocity formula and can be well preserved [Berlin and Anderson, 2007]. Here, however, for a specific knickpoint, the parameter $K'(Q_c^*)$ in the retreat velocity term (Equation 21) relates to the uplift rate that generated the knickpoint. This means that river incision efficiency varies through time and space, in terms of a step function. In the $x - z$ domain, it might be difficult to determine whether all the knickpoints are preserved.

Assuming knickpoint preservation, Equation (21) can be solved:

$$t = \int_0^x \frac{1}{K\prime(Q_c^*) \cdot A^{cm}} dx + t_s = \frac{1}{A_0^{cm} \cdot K\prime(Q_c^*)} \int_0^x [\frac{A_0}{A(x\prime)}]^{cm} dx + t_s = \frac{1}{A_0^{cm} \cdot K\prime(Q_c^*)} \varphi(x) + t_s \quad (23)$$

where t_s indicates a transient signal formed at the base level when $t = t_s$. This implies a boundary condition of $x = 0$ and $z = 0$ at $t = t_s$ [Goren et al., 2014; Rudge et al., 2015]. Equation (23) measures a response time for a knickpoint migration from river outlet to its present location.

Equation (22) can be solved:

$$z = \int_0^t [U(t') + E_c(Q_c^*)]\, dt' + z_s \quad (24)$$

where z_s is a constant term that can be derived by using the boundary condition:

$$z_s = -\int_0^{t_s} [U(t') + E_c(Q_c^*)]\, dt' \quad (25)$$

Assigning Equations (23 and 25) into (24), we derived the closed form analytical solution to the linear model:

$$z = \int_{t_s}^t [U(t') + E_c(Q_c^*)]\, dt' = \int_{t - \frac{1}{A_0^{cm} \cdot K\prime(Q_c^*)} \varphi(x)}^t [U(t') + E_c(Q_c^*)]\, dt' \quad (26)$$

Since K' is usually unknown, a non-dimensional K'-independent uplift history is needed. We followed Goren et al. [2014] to define two new variables:

$$t^* = t \cdot A_0^{cm} \cdot K'(Q_c^*) \quad (27)$$

$$\text{and } U^*(t^*) = [U(t) + E_c(Q_c^*)]/(A_0^{cm} \cdot K'(Q_c^*)) \quad (28)$$

Thus, Equation (26) can be related to a K'-independent uplift history:

$$z(t^*, x) = \int_{t^*-\varphi(x)}^{t^*} U^*(t^{*\prime})\, dt^{*\prime} \quad (29)$$

Hence, Equation (29) represents the knickpoint evolution in the $\varphi - z$ domain and segments between knickpoints are straight lines.

4 A linear inverse scheme to infer tectonic uplift history

The analytical solution provides a linear inverse scheme that takes the river long profiles as input data to infer the relative uplift rate history. According to Equation (29), the present channel profile (at $t = 0$) is:

$$z(x) = \int_{-\varphi(x)}^{0} U^*(t^*)\, dt^* \quad (30)$$

We proposed three steps to infer the uplift history. First, via Equations (16-17), we transformed the river long profiles to $\varphi - z$ plots. A series of cm values were using and the one that minimizes the scatter in the $\varphi - z$ domain was selected [e.g. Goren et al., 2014; Shelef et al., 2018]. Second, we defined knickpoints $[(\varphi_1, z_1), (\varphi_2, z_2), \ldots (\varphi_{N-1}, z_{N-1})]$ to divide the $\varphi - z$ domain into N segments. The basin outlet is identified with $(\varphi_0 = 0, z_0 = 0)$ and the highest channel head is $(\varphi_N = \varphi_{max}, z_N = z_{max})$. These data points are assumed to share a common uplift history (i.e. spatially uniform uplift pattern). Segment j, between $[(\varphi_{j-1}, z_{j-1}), (\varphi_j, z_j)]$, is characterized by a uniform steepness index that shaped the river profile during time interval (t_{j-1}, t_j), where t_j is the time for a transient signal migrating from the river outlet (x_0 or φ_0) to the point (x_j or φ_j). In this way, we can re-write Equation (30) as:

$$z(x_j) = \int_{-\varphi_j}^{0} U^*(t^*)\, dt^* = \sum_{i=1}^{j} U_i^* \cdot (\varphi_i - \varphi_{i-1}) \quad (31)$$

where φ_j equals to t_j^*. U_j^* can be estimated by a linear regression on the data points within the time interval $(\varphi_{j-1}, \varphi_j)$. Consequently, a non-dimensional uplift history, (U_j^*, t_j^*), without any prior information on K', can be derived. Third, conversion from (U_j^*, t_j^*) to a dimensional history (U_j, t_j) by solving equations (27-28), after K' is independently constrained.

The inferred uplift history depends on how to choose the φ interval, which can be evaluated based on the misfit function. Combing the non-dimensional history and Equation (31), we can modelled the channel profiles. We followed Wang et al. [2022] to calculate the elevation misfit between the modelled and actual river profiles:

$$\text{misfit} = \frac{1}{M/N} \sqrt{\sum_{i=1}^{M} (z_i - \widetilde{z_i})^2} \quad (32)$$

where M is the number of pixels in the river profile data. z_i and $\widetilde{z_i}$ are the actual and modelled elevation at the channel node i.

5 Application: linear inversion on the channel profiles of the Dadu River basin

We present an application of the linear inverse scheme to the Dadu River, in the eastern margin of the Tibetan Plateau. The river basin is a transient landscape, characterized by high-elevation, low-relief topography in the interior of the Songpan-Ganze block and steep margins deeply dissected by the major trunk and tributaries of large rivers (Figure 1a). Rock exhumation rates in the region increased dramatically at 9-13 Ma, suggesting synchronous fluvial response to the regional uplift initiated at that time [Clark et al., 2005; Tian et al., 2015]. Another event of the Dadu-Anning capture was dated at the early Pleistocene that the upstream of the paleo Anning River was captured by the trunk of the present Dadu River at Shimian and then flowed into the Sichuan Basin [Clark et al., 2004; Yang et al., 2019; Wang et al., 2021].

We selected five long main trunks distributed in the Dadu River basin (Figure 1a), which was chosen as a case study in Wang et al. [2022]. We extracted the long profiles of these rivers and observed two generations of knickpoints at the elevations of about 1700 and 3000-3500 m (Figure 1b). Adopting $c = 1$ and $m = 0.45$ [Scherler et al., 2017], the generated φ-elevation plots show a uniform trend (Figure 1c). We assumed the number of knickpoints to be 1 to 9 and for each case, we performed 5000 realizations of the inversion with randomly selected positions of knickpoints. For each model run, we modeled river φ-elevation plots via Equation (31) and calculated the elevation misfit by Equation (32). We listed the elevation misfit as a function of the number of assumed knickpoints and presented the non-dimensional uplift history that corresponds to the minimum misfit value at two knickpoints (Figure 1d-e). The results of Figure 1c-e are nearly the same to those in Wang et al. [2022].

In this case, we fixed parameters, $a = 3/2$, $\omega_s = 0.25$, $\omega_b = 0.55$, $\tau_c = 45$ Pa, $k_e = 4.3 \times 10^{-12}$ $\mathrm{m}^{2.5}s^2\mathrm{kg}^{-1.5}$, $k_t = 1000$ $\mathrm{m}^{-7/3}s^{-4/3}\mathrm{kg}$, and $k_w = 15$ $\mathrm{m}^{-0.65}s^{0.55}$ [Dibiase and Whipple, 2011]. Next, we estimated the parameters, R_b and k, based on the monotonic, positive non-linearity between erosion rates with channel steepness:

$$k_s = k_\Phi \cdot E^\Phi \quad (33)$$

Ouimet et al. [2009] reported a data set of $E - k_s$ in the Dadu and adjacent river catchments. A free fit to the data produced the exponent $\Phi = 0.4874$ (Figure 2). Assigning the k_s data of Ouimet et al. [2009] into Equations (18 and 10), we calculated erosion rates and the statistic scaling between the rates and steepness indices. The resulted parameters, Φ and k_Φ, vary a lot for changes in R_b and k (Figure 3).

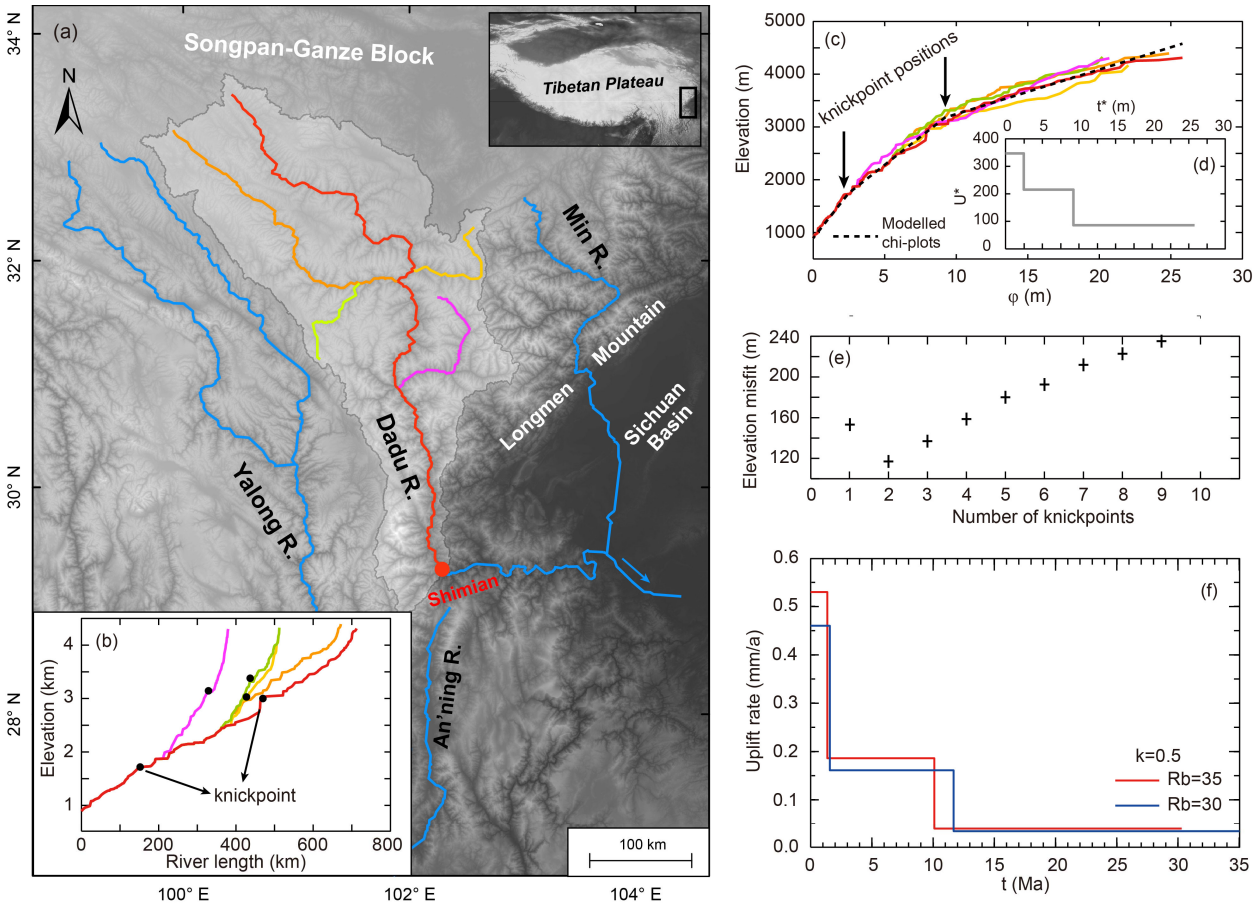

Figure 1. (a) Location of the Dadu River basin. The long, main trunks selected for inversion are in colors. (b) The long profiles of the selected trunk channels, with prominent knickpoints labeled in black dots. (c) The colored, solid lines are the φ-elevation plots of the main trunks and the black, dashed line is the best-fit inferred φ-elevation plot with the history shown in (d). (d) The non-dimensional history of relative uplift rate with the best-fit solution by using two knickpoints. (e) The elevation misfit as a function of the number of division points, based on equation (32). (f) The inferred dimensional uplift history with the same runoff variability but different R_b values.

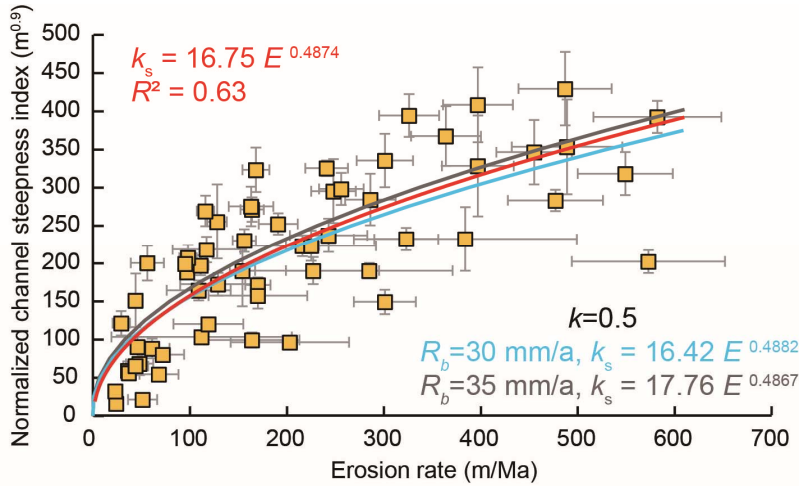

Figure 2. The non-linearity of the measured erosion rates and channel steepness. The data with error bars (1σ uncertainty) are from Ouimet et al. [2009]. Red line indicates a free fit to the dataset. Gray and blue lines show the best fit of Equation (10) through erosion rates, using the same runoff variability but different R_b values.

Figure 3a shows that, when $k \geq 1$ and R_b is no more than 2000 mm/a, the Φ is always below 0.45. Although Φ has the potential to be over 0.45 for much higher runoff, the coefficient k_Φ is getting close to zero (Figure 3b). Figure 3c and e indicates that, as long as $k \leq 0.4$, the Φ is higher than 0.5. If $k \geq 0.6$, the high runoff ($R_b \geq 500$) produces a Φ that is close to 0.48 but $k_\Phi < 10$ (Figure 3e-f). When $k = 0.5$ and $30 \leq R_b \leq 35$, we obtained $\Phi \sim (0.4867, 0.4882)$ and $k_\Phi \sim (16.42, 17.76)$ (Figure 3g-h). This is consistent with the results of the free fit to the $E - k_s$ dataset (Figure 2).

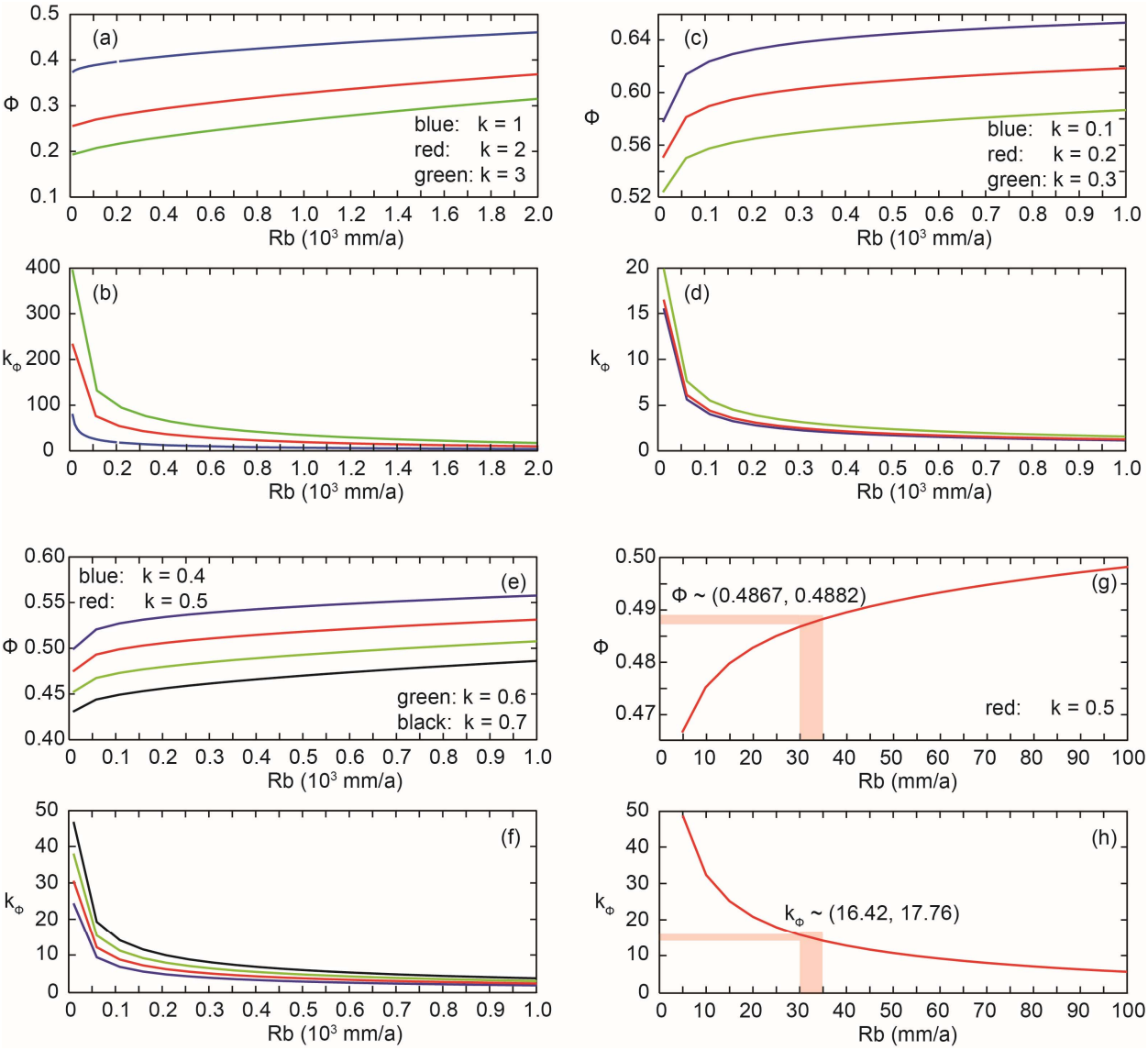

Figure 3. The coefficient (k_Φ) and exponent (Φ) of the erosion rate – channel steepness scaling change as a function runoff (R_b) and its variability (k).

Thus, we fixed $k = 0.5$ and used $R_b = 30$ and 35 to calculate the history of relative uplift rates. Both the two histories nearly show the same trend with two-phase of increase in the uplift rates since the Miocene, i.e. one is at 10-12 Ma (the rate increased from 0.05 to ~0.20 mm/a) and another is at 1.5-2.0 Ma (from 0.20 to 0.45-0.55 mm/a). The inferred history is consistent with the timing of the tectono-geometric events revealed by low temperature studies [e.g. Ouimet, 2007; Tian et al., 2015; Yang et al., 2019]. And, the history produces an average rate of relative uplift to be about 0.25-0.30 mm/a (from 10-12 Ma to the present), which is similar to the incision rates (derived from elevation transects of apatite fission track and Helium ages) along the trunk channel of the Dadu River [Clark et al., 2005].

6 Discussion

6.1 Limitation and assumption

The analytic work we presented here was based on an essential assumption that erosion rate depends on channel slope linearly, i.e. the slope exponent $n = 1$. This assumption relies on the combination of a non-linear relation ($a = 3/2$ in Equation 2) between instantaneous incision rate with shear stress and a Darcy-Weisbach relation ($\alpha = \beta = 2/3$ in Equation 3) between shear stress with channel slope [Howard, 1994]. In the simple SPIM (Equation 1), the non-linearity in the $E - k_s$ scaling is directly parameterized in the non-linear exponent *n* [Whipple and Tucker, 1999]. Although the non-linear *n* could cause complex fluvial dynamics [Royden and Perron, 2013], Wang et al. [2022] developed an inverse model to extract tectonic uplift history based on the assumption of knickpoint preservation. Choosing the same trunk rivers as a case, both Wang et al. [2022] and this study nearly inferred the same dimensional uplift rate histories. Thus, applying a linear *n* in the stochastic-threshold incision model can also solve some inverse problems relating to the non-linear dependence of channel steepness on river erosion rate.

Another limitation is that our model uses constant runoff and variability. In the case study, we obtained runoff of 30-35 mm/a and variability parameter $k = 0.5$ to best match the observed $E - k_s$ scaling. However, for the rivers southeast to the Dadu, the runoff recorded by modern hydrological stations is more than 500 mm/a and $k > 3$ [Scherler et al., 2017]. That might be because that those stations are mainly on large rivers, while the $E - k_s$ dataset are mostly from small-scale tributary catchments of the Dadu River [Ouimet et al., 2009]. It means that the climate parameters that was calibrated via the dataset of small catchments were extrapolated to the inversion on the long, main trunks of the Dadu basin. The inferred history is well consistent with the exhumation history along the trunk of the Dadu River [Clark et al., 2005], which might indicate a consistence in the adjustment response of both trunk and tributary channels to the changes in incision and/or uplift rates. It also implies that the $E - k_s$ scaling at 10^3-10^4 yr scale can be extrapolated to a long time scale of $>10^6$ yr. Despite the global climate changes since 2-4 Ma [Zhang et al., 2001], both numerical and analytical models show that the high-frequency oscillations are not expected to leave significant effects on the topography of bedrock fluvial channels [Goren et al., 2016].

6.2 Whether knickpoints can be preserved

Our analytical solution and inverse method are both based on the premise of no knickpoint merge. Here, we demonstrated that, under the linear stochastic-threshold incision model, all the knickpoints can be well preserved. Taking the transformation of Equations (17, 27 and 28), we can write:

$$\frac{\partial z}{\partial t} = \frac{\partial z}{\partial t^*} \cdot \frac{dt^*}{dt} = \frac{\partial z}{\partial t^*} \cdot A_0^{cm} \cdot K'(Q_c^*) \quad (34)$$

$$\frac{\partial z}{\partial x} = \frac{\partial z}{\partial \varphi} \cdot \frac{d\varphi}{dx} = \frac{\partial z}{\partial \varphi} \cdot [\frac{A_0}{A(x\prime)}]^{cm} \quad (35)$$

Substituting Equations (34-35) into (19):

$$\frac{\partial z}{\partial t^*} \cdot A_0^{cm} \cdot K'(Q_c^*) + K'(Q_c^*) \cdot A(x)^{cm} \cdot \frac{\partial z}{\partial \varphi} \cdot [\frac{A_0}{A(x)}]^{cm} = U(t) + E_c(Q_c^*) \quad (36)$$

Our approach resolved knickpoint kinematics in a Lagrangian reference frame, which implies that, along a channel segment between two adjacent knickpoints, K' should be a constant. Thus, Equation (36) can be re-arranged as:

$$\frac{\partial z}{\partial t^*} + \frac{\partial z}{\partial \varphi} = \frac{U(t)+E_c}{A_0^{cm} \cdot K\prime} = U^*(t^*) \quad (37)$$

One of the characteristic equations of Equation (37) is:

$$d\varphi/dt^* = 1 \quad (38)$$

Thus, taking the transformation of Equations (17, 27 and 28), the transient signals (knickpoints) migrates at the same velocity in the φ-elevation domain. Thus, our inverse scheme based on the analytical solution to the linear STIM can deal with inverse problems relating to a nonlinear $E - k_s$ scaling, without the assumption of knickpoint preservation.

Notably, we do not mean that all the nonlinear $E - k_s$ cases can be resolved by the simple stochastic-threshold model. Nevertheless, a combination of this approach and previous analytical studies on $n \neq 1$ [e.g. Royden and Perron, 2013; Wang et al., 2022] could produce better understandings on more complex fluvial dynamics. Besides, incorporating our analytical procedures into forward and inverse tectonic – fluvial landscape evolution models [e.g. Fox et al., 2015; Gallen and Fernández-Blanco, 2021; Steer et al. 2021] has the potential to significantly expedite the model run speed and to make these models more efficient and accurate.

7 Conclusion

In this contribution, we presented analytical solutions to the simple stochastic-threshold incision model equation. The solution to the steady-state equation of the model produces a φ-elevation transformation to river long profile. Under the assumptions of a linear slope exponent and the timely dependent uplift, we derived a closed-form analytical solution to the transient state equation. This solution allows to relate the topography along fluvial channels to the history of the relative uplift rate through time. Based on the analytical analysis, we developed a linear inversion scheme to retrieve the tectonic uplift rate history from river long profiles. We applied the inverse method to the Dadu River basin where channel steepness indices scale with catchment erosion rates non-linearly. We inferred a history with two-stage increases in the

uplift/incision rates since the late Miocene, which is consistent with the exhumation history recorded by low-temperature thermochronology. Our analytical procedures thus provide powerful tools for understanding the transient behavior of bedrock channel evolution.

Acknowledgments

We appreciate the work of Dibiase and Whipple. [2011] and Goren et al. [2014], from which the first author got inspiration to conduct this study. This study was supported by the National Science Foundation of China (42172242).

Open Research

The 90 m Shuttle Radar Topography Mission (SRTM) DEM (digital elevation model) data can be freely downloaded at https://earthexplorer.usgs.gov/ for the analysis on fluvial topography of the Dadu River basin. There is no codes sharing issues, as all the results can be reproduced by solving the equations in the text. We declare no conflict of interest.

References

Berlin, M.M., and Anderson, R.S. (2007). Modeling of knickpoint retreat on the Roan Plateau, western Colorado. J. Geophys. Res., 112, F03S06, doi:10.1029/2006JF000553.

Clark, M.K., House, M.A., Royden, L.H., Whipple, K.X., Burchfiel, B.C., Zhang, X., and Tang, W., (2005). Late Cenozoic uplift of southeastern Tibet. Geology, 33(6): 525‐528. doi: https://doi.org/10.1130/G21265.1

Clark, M.K., Schoenbohm, L.M., Royden, L.H., Whipple, K.X., Burchfiel, B.C., Zhang, X., Tang, W., Wang, E., and Chen, L., (2004). Surface uplift, tectonics, and erosion of eastern Tibet from large-scale drainage patterns. Tectonics 23, TC1006.

DiBiase, R. A., and K. X. Whipple (2011). The influence of erosion thresholds and runoff variability on the relationships among topography, climate, and erosion rate, J. Geophys. Res., 116, F04036, doi:10.1029/2011JF002095.

Fox, M., Bodin, T., and Shuster, D.L. (2015). Abrupt changes in the rate of Andean Plateau uplift from reversible jump Markov Chain Monte Carlo inversion of river profiles. Geomorphology 238:1–14.

Gallen, S. F., and Fernández-Blanco, D. (2021). A new data-driven Bayesian inversion of fluvial topography clarifies the tectonic history of the corinth rift and reveals a channel steepness threshold. J. Geophys. Res. Earth, 126, e2020JF005651. https://doi.org/10.1029/2020JF005651.

Goren, L. (2016). A theoretical model for fluvial channel response time during time-dependent climatic and tectonic forcing and its inverse applications, Geophys. Res. Lett., 43, 10,753‐10,763, doi:10.1002/2016GL070451.

Goren, L., Fox, M., and Willett, S.D. (2014). Tectonics from fluvial topography using formal linear inversion: theory and applications to the Inyo Mountains, California. J. Geophys. Res. Earth 119:1651–1681.

Goren, L., Fox, M., and Willett, S. D. (2021). Linear Inversion of Fluvial Long Profiles to Infer Tectonic Uplift Histories, Reference Module in Earth Systems and Environmental Sciences, Elsevier, ISBN 9780124095489, https://doi.org/10.1016/B978-0-12-818234-5.00075-4.

Harel, M.-A., Mudd, S.M., and Attal, M. (2016). Global analysis of the stream power law parameters based on worldwide 10Be denudation rates. Geomorphology 268, 184-196. doi:10.1016/j.geomorph.2016.05.035

Harkins, N., Kirby, E., Heimsath, A., Robinson, R., and Reiser, U. (2007). Transient fluvial incision in the headwaters of the Yellow River, northeastern Tibet, China. J. Geophys. Res. Earth 112: F03S04.

Johnson, J.P., and Whipple, K.X., (2007). Feedbacks between erosion and sediment transport in experimental bedrock channels: earth Surface Processes and Landforms. Earth Surf. Process. Landforms 32, 1048-1062.

Hilley, G.E., Porder, S., Aron, F., Baden, C.W., Johnstone, S.A., Liu, F., Sare, R., Steelquist, A., and Young, H.H., (2019). Earth's topographic relief potentially limited by an upper bound on channel steepness. Nat. Geosci. 12: 828–832.

Howard, A. D. (1994). A detachment limited model of drainage-basin evolution, Water Resour. Res., 30(7), 2261‐2285, doi:10.1029/94WR00757.

Howard, A.D., and Kerby, G. (1983). Channel changes in badlands. Geol. Soc. Am. Bull. 94, 739-752.

Kirby, E., and Whipple, K.X. (2012). Expression of active tectonics in erosional landscapes. J. Struct. Geol. 44:54–75. http://dx.doi.org/10.1016/j.jsg.2012.07.009

Lague, D. (2014). The stream power river incision model: evidence, theory and beyond. Earth Surf. Process. Landf. 39, 38–61.

Lague, D., Hovius, N. and Davy, P. (2005). Discharge, discharge variability, and the bedrock channel profile, J. Geophys. Res., 110, F04006, doi:10.1029/2004JF000259.

Montgomery, D. R., and K. B. Gran (2001). Downstream variations in the width of bedrock channels, Water Resour. Res., 37(6), 1841‐1846, doi:10.1029/2000WR900393.

Ouimet, W.B., Whipple, K.X., and Granger, D.E. (2009). Beyond threshold hillslopes: channel adjustment to base-level fall in tectonically active mountain ranges. Geology 37(7), 579–582. http://dx.doi.org/10.1130/G30013A.1.

Perron, J.T., and Royden, L. (2013). An integral approach to Bedrock River profile analysis. Earth Surf. Process. Landf. 38:570–576. http://dx.doi.org/10.1002/esp.3302.

Pritchard, D., Roberts, G.G., White, N.J., and Richardson, C.N. (2009). Uplift histories from river profiles. Geophys. Res. Lett., 36, L24301. doi:10.1029/2009GL040928

Refice, A., Giachetta, E., and Capolongo, D. (2012). Signum: a MATLAB, tin-based landscape evolution model. Computers and Geosciences 45(0): 293‐303.

Royden, L., and Perron, J.T. (2013). Solutions of the stream power equation and application to the evolution of river longitudinal profiles. J. Geophys. Res. Earth 118 (2):497–518. http://dx.doi.org/10.1002/jgrf.20031.

Rudge, J.F., Roberts, G.G., White, N.J., and Richardson, C.N. (2015). Uplift histories of Africa and Australia from linear inverse modeling of drainage inventories. J. Geophys. Res. Earth 120, 894–914.

Scherler, D., DiBiase, R.A., Fisher, G.B., and Avouac, J.-P. (2017). Testing monsoonal controls on bedrock river incision in the Himalaya and Eastern Tibet with a stochastic-threshold stream power model, J. Geophys. Res. Earth Surf., 122, 1389‐1429, doi:10.1002/2016JF004011.

Snyder, N.P., Whipple, K.X., Tucker, G.E., and Merritts, D.J., (2003). Importance of a stochastic distribution of floods and erosion thresholds in the bedrock river incision problem. J. Geophys. Res. 108, 2117.

Steer, P. (2021). Short communication: Analytical models for 2D landscape evolution. Earth Surf. Dynam., 9(5), 1239-1250.

Tian, Y., Kohn, B.P., Hu, S., and Gleadow, A.J.W., (2015). Synchronous fluvial response to surface uplift in the eastern Tibetan Plateau: Implications for crustal dynamics, Geophys. Res. Lett., 42, 29‐35, https://doi.org/10.1002/2014GL062383.

Tucker, G. E. (2004). Drainage basin sensitivity to tectonic and climatic forcing: Implications of a stochastic model for the role of entrainment and erosion thresholds, Earth Surf. Processes Landforms, 29(2), 185‐205, doi:10.1002/esp.1020.

Tucker, G., Lancaster, S., Gasparini, N., and Bras, R. (2001). The channelhillslope integrated landscape development model (child). In Landscape Erosion and Evolution Modeling, Harmon RS, Doe WW III (eds). Springer: New York; 349‐388.

Wang, Y., Goren, L., Zheng, D., and Zhang, H., (2022). Short communication: Forward and inverse analytic models relating river long profile to tectonic uplift history, assuming a nonlinear slope‐erosion dependency, Earth Surf. Dynam., 10, 833‐849, https://doi.org/10.5194/esurf-10-833-2022.

Wang, Y., Liu, C., Zheng, D., Zhang, H., Yu, J., Pang, J., Li, C., and Hao, Y., (2021). Multistage exhumation in the catchment of the Anninghe River in the SE Tibetan Plateau: Insights from both detrital thermochronology and topographic analysis, Geophys. Res. Lett., 48, e2021GL092587, https://doi.org/10.1029/2021GL092587.

Whipple, K. X. (2009). The influence of climate on the tectonic evolution of mountain belts, Nat. Geosci., 2(10), 730, doi:10.1038/ngeo638.

Whipple, K.X., and Tucker, G.E. (1999). Dynamics of the stream power river incision model: Implications for height limits of mountain ranges, landscape response timescales and research needs, J. Geophys. Res., 104, 17,661–17,674.

Whipple, K.X., and Tucker, G.E. (2002). Implications of sediment-flux-dependent river incision models for landscape evolution. Journal of Geophysical Research, Solid Earth 107(B2). https://doi.org/10.1029/2000JB000044.

Yang, R., Suhail, H.A., Gourbet, L., Willett, S.D., Fellin, M.G., Lin, X., Gong, J.F., Wei, X.C., Maden, C., Jiao, R.H., and Chen, H.L., (2019). Early Pleistocene drainage pattern changes in Eastern Tibet: Constraints from provenance analysis, thermochronometry, and numerical modeling, Earth Planet. Sc. Lett., 531, 115955, https://doi.org/10.1016/j.epsl.2019.115955.

Zhang, H., E. Kirby, J. Pitlick, R. S. Anderson, and P. Zhang (2017). Characterizing the transient geomorphic response to base-level fall in the northeastern Tibetan Plateau, J. Geophys. Res. Earth Surf., 122, doi:10.1002/2015JF003715.

Zhang, P., Molnar, P., and Downs, W.R., (2001). Increased sedimentation rates and grain sizes 2‐4 Myr ago due to the influence of climate change on erosion rates. Nature, 410, 891‐897.